Sparse Reconstruction Methods in RF Tomography for Underground Imaging

Lorenzo Lo Monte
General Dynamics Information Technology
Wright-Patterson AFB, OH, USA
Lorenzo.Lomonte.ctr@wpafb.af.mil

Jason T. Parker
Air Force Research Laboratory / Sensors Directorate
Wright-Patterson AFB, OH, USA
Jason.Parker@wpafb.af.mil

***Abstract*— Underground imaging involving RF Tomography is generally severely ill-posed posed. Tikhonov Regularization is perhaps the most common method to address this ill-posedness. The proposed methods are based upon the realistic assumptions that targets (e.g. tunnels) are sparse and clustered in the scene, and have known electrical properties. Therefore, we explore the use of alternative regularization strategies leveraging sparsity of the signal and its spatial gradient, while also imposing physically-derived amplitude constraints. By leveraging this prior knowledge, cleaner scene reconstructions are obtained.**

I. INTRODUCTION

The response to calamities, relief activities and asymmetric threats for both civilian and military bodies has increased the demand for close-in and distributed sensing of underground scenes. The situational awareness needed by decision makers is supplied by delivering timely, persistent, and actionable images of the area of interest, regardless of the complexity of the background and the disposition of sensors. To achieve this goal, imaging using RF Tomography may be a suitable choice. This imaging technique arises from classical diffraction tomography and inverse scattering theories [1-3]. RF Tomography is a method for the imaging of high-contrast dielectric / conducting extended targets under highly attenuated, highly cluttered, complex environments, based upon an arbitrarily *distributed* network of low-cost, narrowband, configurable and automated RF sensors. These sensors are placed on top, above, or into the ground at *arbitrary* positions. In a preliminary stage, sensors accurately identify their position, orientation and time reference. Once the calibration phase is concluded, a pre-determined set of transmitters radiates a known waveform using a suitable polarization. The probing wave impinges upon dielectric / conducting targets, thus generating a scattered wave-field. The distributed receivers collect samples of the electric field, mitigate clutter and the direct path, and store the information concerning only the scattered field. In the next iteration, a different set of transmitters is activated, or different waveforms / polarizations are used. Subsequently, the collected data is relayed to the command and control post for processing and imaging. The system operates using ultra-narrowband, adaptive waveforms, thus ensuring low noise, low frequency dispersion, and an economic architecture.

RF Tomography for underground imaging has been introduced mathematically in [4-5]. In these works, a linear forward model of the scattering process is constructed, and data is collected to form a matrix equation. The image of the scene is generally retrieved by matrix inversion, with acceptable results. However, in most cases underground targets, such as tunnels, weapon caches, or UGFs, can be assumed to be sparse (in terms of voxels), clustered, and having predictable electrical properties. For instance, a typical UGF can be described as the interconnection of few (i.e., sparse) hollow (i.e. having relative dielectric permittivity equal to unity) cylinders (i.e. having some minimal spatial extension). This accrued knowledge is generally not exploited in classical inversion schemes. In this work, we propose the adaptation of recent sparse regularization techniques to the particular case of RF tomography for belowground imaging. In particular, we formulate two suitable inversion algorithms based upon the assumption of sparse, clustered and bounded data, and we compare the results with classical inversion algorithms, which rely on Tikhonov regularization.

II. FORWARD MODEL

RF tomography can be described by considering the 3D transmitter-receiver geometry depicted in Fig. 1. For simplicity, a set of N electrically small tunable dipoles (length l) acting as transmitters, and a set of M electrically small tunable dipoles acting as receivers represent the distributed sensor network in RF tomography. The extension to more complicated radiator (corresponding to more directive radiation patterns) can be constructed as superposition of elementary small dipoles, but it will not be shown in this brief description. The *n*-th transmitting dipole, of length *l,* is located at position $\mathbf{r}_n^a$, and has current amplitude, phase and direction described by the 3D complex vector $\mathbf{a}_n$. The *m*-th receiving dipole is located at position $\mathbf{r}_m^b$, and directed along the unit-norm vector $\hat{\mathbf{b}}_m$. Each transmitter emits a monochromatic signal with frequency f.

We assume the air-earth interface to be flat; however, the problem of non-flat surfaces can be solved as well (at additional complexity [7]). In this context, the air half-space is modeled as free-space medium, while the ground half-space is modeled as an homogeneous medium with background relative dielectric permittivity ε_D, background conductivity σ_D, and magnetic permeability μ_0. The dielectric/conducting targets are assumed to reside in a pre-determined investigation domain *D*, which lies in the interior of the gorund half-space. A scattering body located at position $\mathbf{r}'$ inside D is described by a deviation in the relative dielectric permittivity $\varepsilon_r(\mathbf{r}')$ and the conductivity $\sigma(\mathbf{r}')$. Unlike other applications, the detection of targets does not require the discrimination between dielectric and conducting bodies. Hence, for convenience, we can define a complex-valued *contrast function*:

$$V(\mathbf{r}') = \varepsilon_r(\mathbf{r}') - \varepsilon_D + j\left(\sigma(\mathbf{r}') - \sigma_D\right)/2\pi f\varepsilon_0 \quad (1)$$

where ε_0 is the dielectric permittivity of free space. Rather than using a single transmitter, we prefer to irradiate the scene using a set of s simultaneously activated transmitters, represented by the index set Γ_S. Following the derivations reported in [4], the contrast function $V(\mathbf{r}')$ can be related to the measured total field at the receiver side, due to simultaneous transmission of s transmitters operating at angular frequency ω, $E\left(\mathbf{r}_m^b, \Gamma_S, \mathbf{b}_m, f\right)$, via the relation:

$$E\left(\mathbf{r}_m^b, \Gamma_S, \hat{\mathbf{b}}_m, f\right) = \overbrace{\hat{\mathbf{b}}_m^T \cdot \mathbf{Z}\left(\mathbf{r}_m^b, \Gamma_S, \mathbf{b}_m, f\right)}^{\text{nonlinear terms, multipath, noise}}$$
$$\overbrace{j2\pi f\mu_0 l \hat{\mathbf{b}}_m^T \cdot \left[\sum_{n\in\Gamma_S} \underline{\mathbf{G}}\left(\mathbf{r}_m^b, \mathbf{r}_n^a, f\right)\cdot \mathbf{a}_n\right]}^{\text{direct path}} + \quad (2)$$
$$\left.\begin{aligned} & j2\pi f\mu_0 k_0^2 l \iiint_D \hat{\mathbf{b}}_m^T \cdot \underline{\mathbf{G}}\left(\mathbf{r}_m^b, \mathbf{r}', f\right)\cdot \\ & \left[\sum_{n\in\Gamma_S} \underline{\mathbf{G}}\left(\mathbf{r}', \mathbf{r}_n^a, f\right)\cdot \mathbf{a}_n\right] V(\mathbf{r}')\, d\mathbf{r}' \end{aligned}\right\} \text{scattered field}$$

The 3×3 matrix $\underline{\mathbf{G}}$ is the Green's dyadic for the half-space geometry, and it is assumed known: explicit formulas are provided in [2-5]. The vector $\mathbf{Z}$ represents noise and the superposition of effects that are not accounted for by the Born approximation, which has been used to derive (2): We will neglect these terms in order to arrive at a tractable linear model. This approximated formula represents the *Forward Model* in RF Tomography in its simplest form.

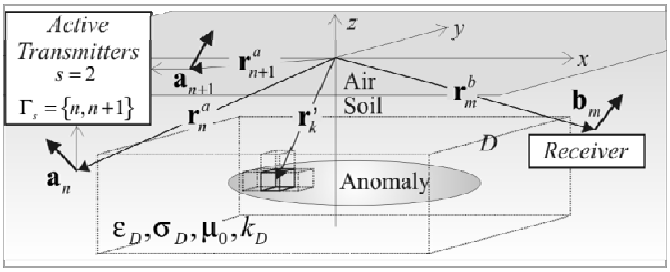

Figure 1: Geometry of RF tomography.

III. Discretization

The continuous equation in (2) can be discretized using the method of moments. For simplicity we will use both weighting functions and testing functions to be δ Dirac. Therefore, we collect a discrete set of measurements by varying $\mathbf{r}_m^b, \hat{\mathbf{b}}_m, s, f$ to form a measurement vector $\mathbf{e}$. Moreover, the domain D is discretized into K voxels, each one represented by a δ-Dirac located at $\mathbf{r}'_k$, so that we can define a contrast vector $\mathbf{v} = \left\{V\left(\mathbf{r}'_k\right)\right\}$ (see Fig. 1). According to the classical Riemann summation, the integral operation on V can be discretized into a matrix $\underline{\mathbf{L}}$, provided that the field inside each voxel *k* is relatively constant. The contribution in (2) representing the direct path can be also discretized in vector $\mathbf{p}$. Therefore, the forward model can be approximated in discrete form by $\mathbf{e} \cong \underline{\mathbf{L}}\mathbf{v} + \mathbf{p}$. By denoting the scattered field data as $\mathbf{s} = \mathbf{e} - \mathbf{p}$, the forward model of RF Tomography can be written in matrix equation:

$$\mathbf{s} = \underline{\mathbf{L}}\mathbf{v} \quad (3)$$

Generally, each entry of $\mathbf{s}$ has extremely low value; therefore, slight errors on both $\mathbf{e}$ or $\mathbf{p}$ dramatically change the value of $\mathbf{s}$. One strategy to mitigate the error in $\mathbf{s}$ is to remove the direct-path coupling before the measurements are taken, i.e. $\mathbf{p} \cong \mathbf{0}$. This task is accomplished by either rotating Tx and Rx pairs [5], or by using simultaneously activated transmitters [6]. Regardless of how the direct path is mitigated, residual errors will inevitably remain. We shall approximate these residual errors with an unknown additive perturbation $\mathbf{n}$ to the scattered field measurements $\mathbf{s}$.

IV. Inversion Procedures

In principle, the estimation of $\mathbf{v}$ can be performed as:

$$\hat{\mathbf{v}} \cong \underline{\mathbf{L}}^{\dagger}\mathbf{s} \quad (4)$$

where $\underline{\mathbf{L}}^{\dagger}$ represents a suitable pseudoinverse of $\underline{\mathbf{L}}$. In RF Tomography, estimating $\mathbf{v}$ is generally a hard task for the following reasons:

- The number of collected samples is generally much smaller than the number of voxels of the scene. Therefore, the matrix equation (3) is severely

underdetermined, implying that there exist infinite solutions.

- The matrix $\underline{\mathbf{L}}$ is also very ill-conditioned and may include modeling errors.
- Both vectors $\mathbf{e}$ and $\mathbf{p}$ are affected by noise and clutter, and their difference $\mathbf{s}$ may be extremely low, since in some cases the direct path is 50-60 dB higher than the scattered field itself. Therefore, the per-sample SNR for $\mathbf{s}$ may be as low as zero dB.

To properly retrieve $\mathbf{v}$ one needs to use regularized solutions. Classical regularization methods belong to the so-called class of L_2 norm minimization [2]. For example, the ridge regression, or Tikhonov regularization method in its simplest form can be written as [2]:

$$\arg\min \left\| \underline{\mathbf{L}}\mathbf{v} - \mathbf{s} \right\|_2^2 + \alpha \left\| \mathbf{v} \right\|_2^2 \tag{5}$$

The solution for this minimization problem can be given in closed form, and recovers a solution $\mathbf{v}$ with constrained energy. However, reconstructions based on L_2 norm minimization are generally very smooth, present high side lobes, artifacts, and very low resolution, especially when the number of samples is low. To increase the image quality, one can exploit some prior knowledge on $\mathbf{v}$ such as:

- In tunnel and UGF detection, the entries of $\mathbf{v}$ should be between 0 (i.e., no target) and the difference between the background and the air.
- Since targets in the scene are sparse, the non-zero elements of $\mathbf{v}$ should be a few, although we cannot know *a priori* the exact number of non-zero elements.
- Targets are generally spatially extended (i.e., clustered).

V. Constrained L_1 and L_2 Norms

One way to account for this prior knowledge of $\mathbf{v}$ is to solve the following minimization problem:

$$\arg\min \left\| \underline{\mathbf{L}}\mathbf{v} - \mathbf{s} \right\|_2^2 + \alpha \left\| \mathbf{v} \right\|_1^1 + \beta \left\| \mathbf{v} \right\|_2^2 \tag{6}$$

$$\text{subject to: } \tau_{\min} \le \left| \left(\mathbf{v} \right)_i \right| \le \tau_{\max} \quad i = 1 \ldots K \tag{7}$$

where α, β are constant weights that need to be opportunely determined, $\tau_{\min}$ and $\tau_{\max}$ represent the minimum and maximum absolute value that each voxel can have (usually $\tau_{\min} = 0$ and $\tau_{\max} = 1.5 \times \varepsilon_D$), and $\left(\mathbf{v} \right)_i$ denotes the *i*-th element of $\mathbf{v}$.

In fact, the L_1 penalty promotes solutions having a small number of non-zero elements, i.e., reduces the number of required samples, and decreases sidelobes and artifacts. Furthermore, the condition on the elements of $\mathbf{v}$ guarantees realistic values of the contrast functions, and distributes the energy of the image to weaker voxels. Finally, the small penalty for the L_2 norm prevents the concentration of the energy to single pixels, thus favoring extended objects in the reconstruction.

The problem could be solved using the interior point method [12], or other sparse regularization algorithms such as LARS [9]. However, by recasting (6) as

$$\begin{aligned} &\arg\min \left\| \tilde{\underline{\mathbf{L}}}\mathbf{v} - \tilde{\mathbf{s}} \right\|_2^2 + \beta \left\| \mathbf{v} \right\|_1^1 \\ &\tilde{\underline{\mathbf{L}}} = \begin{bmatrix} \underline{\mathbf{L}} \\ \sqrt{\alpha}\underline{\mathbf{I}} \end{bmatrix}, \tilde{\mathbf{s}} = \begin{bmatrix} \mathbf{s} \\ \mathbf{0} \end{bmatrix} \end{aligned} \tag{8}$$

we can then use the Fast Iterative Shrinking Thresholding Algorithm (FISTA) [10-11], which is much faster with respect to other methods and shows quadratic convergence. The iterations in FISTA can be summarized as follows. At the first step, two variables are initialized, i.e. $\tilde{\mathbf{v}}^{(0)} = \mathbf{v}^{(0)} = \mathbf{0}$ and $t^{(0)} = 1$. The next step of the solution is computed using the following recursive formula:

$$\tilde{\mathbf{v}}^{(n+1)} = T\left(\mathbf{v}^{(n)} + \frac{t^{(n)} - 1}{t^{(n+1)}} \left(\mathbf{v}^{(n)} - \mathbf{v}^{(n-1)} \right) \right) \tag{9}$$

where the shrinking parameter t is given by:

$$t^{(n+1)} = \frac{1}{2}\left(1 + \sqrt{1 + 4\left(t^{(n)} \right)^2} \right), \tag{10}$$

the operator $T\left(\mathbf{x} \right)$ is

$$T\left(\mathbf{x} \right) = S_\beta \left[\mathbf{x} + \tilde{\underline{\mathbf{L}}}^H \left(\tilde{\mathbf{s}} - \tilde{\underline{\mathbf{L}}}\mathbf{x} \right) \right], \tag{11}$$

and the operator $S_\beta \left(\mathbf{z} \right)$ is defined as

$$S_\beta \left(\mathbf{z} \right) = \begin{cases} \left[\left(\mathbf{z} \right)_i - \beta \right] \exp\left(j \angle \left(\mathbf{z} \right)_i \right) & \left| \left(\mathbf{z} \right)_i \right| > \beta \\ 0 \quad \text{otherwise} \end{cases} \tag{12}$$

where the operator $\angle$ returns the phase of the complex number, expressed in radiant. Finally, we modify the standard FISTA algorithm by projecting the estimated $\tilde{\mathbf{v}}^{n+1}$ onto the set of $\mathbf{v}$ satisfying (7), thus giving the actual (feasible) value of $\mathbf{v}^{(n+1)}$. The iteration is stopped when the residual is less that a pre-determined value.

VI. Constrained L_1 and TV Norms

Another minimization procedure that accounts for the prior knowledge of the solution $\mathbf{v}$ can be formulated as follows:

$$\begin{aligned} &\arg\min \left\| \underline{\mathbf{L}}\mathbf{v} - \mathbf{s} \right\|_2^2 + \alpha \left\| \mathbf{v} \right\|_{1S} + \beta \left\| \mathbf{v} \right\|_{TV} \\ &\text{subject to: } \tau_{\min} \le \left| \left(\mathbf{v} \right)_i \right| \le \tau_{\max} \quad i = 1 \ldots K \end{aligned} \tag{13}$$

where

$$\|\mathbf{v}\|_{1S} = \sum_{i=1}^{K}\left(\sqrt{(\mathbf{v})_i^2 + \delta^2}\right), \|\mathbf{v}\|_{TV} = \left\|\sqrt{\left(\nabla|\mathbf{v}|\right)^2 + \delta^2}\right\|_1 \quad (14)$$

represent the smoothed L_1 norm (assuming δ to be a small number), and the smoothed Total Variation norm. The use of differentiable penalty functionals allows us to take advantage of simple and fast-converging algorithms, such as the one described in this section. Note that the gradient operator can be opportunely defined as a matrix operator acting on $|\mathbf{v}|$, i.e. $\nabla|\mathbf{v}| \cong \underline{\mathbf{D}}|\mathbf{v}|$; for details, see [13]. The minimization problem in (13) incorporates several advantages:

- The TV penalty promotes solutions whose amplitudes vary minimally throughout the image. This penalization tends to promote connected solutions. The addition of δ renders the penalty function differentiable.
- The L_1 penalty promotes solutions having a small number of non-zero elements
- The amplitude constraint on $|\mathbf{v}|$ guarantees realistic values of the contrast functions, and distributes the energy of the image to weaker voxels.

To solve the optimization problem in (13), we can take advantage of an efficient iterative algorithm discussed in [13]. After initializing the search vector $\tilde{\mathbf{v}}^{(0)} = \mathbf{v}^{(0)} = \mathbf{0}$, the next iteration is found by solving the following matrix equation:

$$\underline{\tilde{\mathbf{H}}}\left(\mathbf{v}^{(n)}\right)\tilde{\mathbf{v}}^{(n+1)} = (1-\gamma)\underline{\tilde{\mathbf{H}}}\left(\mathbf{v}^{(n)}\right)\mathbf{v}^{(n)} + 2\gamma\underline{\mathbf{L}}^H\mathbf{s} \quad (15)$$

where $0 \le \gamma \le 1$ [14], although we will use $\gamma = 0.5$, and the hessian $\underline{\tilde{\mathbf{H}}}$ is computed as follows:

$$\underline{\tilde{\mathbf{H}}}\left(\mathbf{v}^{(n)}\right) \triangleq 2\underline{\mathbf{L}}^H\underline{\mathbf{L}} + \alpha\underline{\mathbf{A}} + \beta\underline{\mathbf{F}}^H\underline{\mathbf{D}}^H\underline{\mathbf{B}}\underline{\mathbf{D}}\underline{\mathbf{F}} \quad (16)$$

$$\underline{\mathbf{A}}(\mathbf{v}) = \left[diag\left(\left(\left|(\mathbf{v}_i)\right|^2 + \delta^2\right)^{-1/2}\right)\right] \quad (17)$$

$$\underline{\mathbf{B}}(\mathbf{v}) = \left[diag\left(\left(\left|\left(\mathbf{D}|\mathbf{v}|\right)_i\right|^2 + \delta^2\right)^{-1/2}\right)\right] \quad (18)$$

$$\underline{\mathbf{F}}(\mathbf{v}) = diag\left[\exp\left(-j\angle(\mathbf{v})_i\right)\right] \quad (19)$$

where the operator $diag(\bullet)$ denotes a diagonal matrix whose *i*-th diagonal element is given by the expression inside the brackets. The computation of (15) can be easily solved using a preconditioned conjugate gradient algorithm. Once $\tilde{\mathbf{v}}^{(n+1)}$ is found, a feasible value of $\mathbf{v}^{(n+1)}$ is chosen by projecting $\tilde{\mathbf{v}}^{(n+1)}$ onto the space of $\mathbf{v}$ satisfying the hard constraint.

VII. Simulations and Results

A simulated scene has been developed to benchmark the proposed algorithms with a classical Tikhonov regularization. A set of 6 transmitters and 6 receivers are encircling the area (see Fig. 2). Transmitters and receivers are electrically small dipoles with unitary dipole moment. However, the direction of each Tx-Rx pair is selected in such a way that the direct-path coupling is mitigated, as described in [5]. Using this strategy, the collected field at the receiver is approximately composed of scattered fields only. The target is a L-shaped tunnel, of circular radius of 1m. The tunnel resides at the depth of 30m. The background dielectric permittivity is $\varepsilon_D = 9$ and the background conductivity is $\sigma_D = 5\times10^{-4}$ [S/m]. The frequency of operation varies from 4MHz to 7MHz, with steps of 0.25MHZ. The forward scattering is computed using the FDTD simulator GPRMAX [8]. This simulator has been extensively tested and used as a benchmark in many scientific articles. Although no artificial noise is added to the collected data, we can assume that the nonlinear scattering, the finite discretization of the scene, and the imperfect direct-path cancellation represent a significant source of error in the measurements. To reduce the dimension of the matrix, we assume approximately known the depth of the tunnel location, so that the region D is confined in the space:

$$D = \{-20 \le x \le 20, -20 \le y \le 20, -32 \le z \le -28\} \quad (20)$$

Each voxel is 1m^3. Therefore, matrix $\underline{\mathbf{L}}$ has a reasonable size of 360×8405. Slices of reconstructions at depth 30m are shown for three cases. In Fig 3, we plotted the reconstruction obtained by solving (5) the classical Tikhonov regularization. In Fig 4, we solved (8) using FISTA with $\beta \cong \alpha/50$. Finally, we solved (13) using the method described in Section VI with $\alpha \cong \beta$. Note that the absolute values of the parameters α and β have been chosen empirically, since they change according to $\|\mathbf{s}\|$ and $\|\underline{\mathbf{L}}\|$.

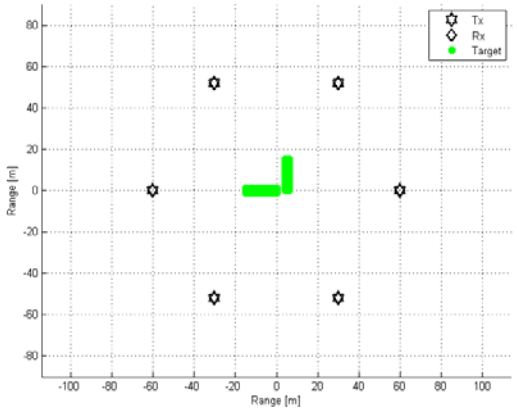

Figure 2: Geometry of the problem

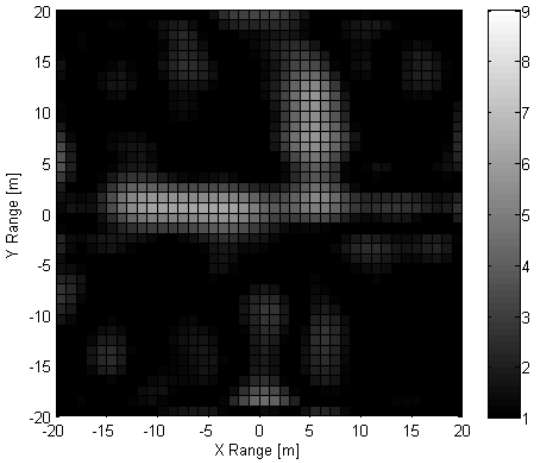

Figure 3: Reconstructed image using Tikhonov

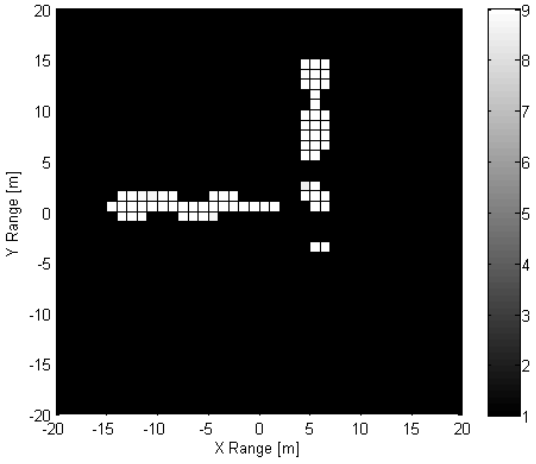

Figure 4: Reconstructed Image using L1 and L2 (FISTA)

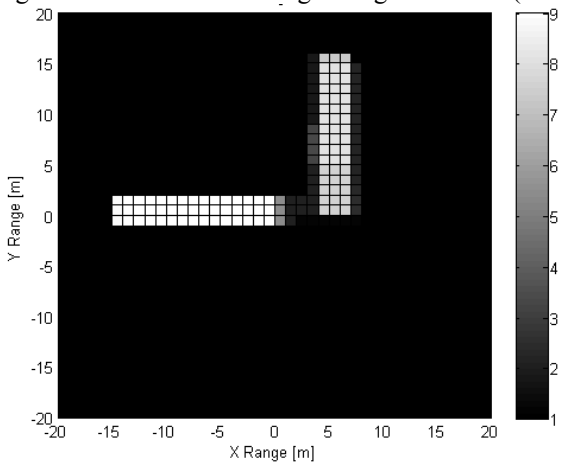

Figure 5: Reconstructed Image using L1 and TV

VIII. CONCLUSION

We expressed the problem of RF tomography for underground imaging in matrix form. The solution of the matrix equation, which represents the image of the underground scene, is sought using improved inversion procedures. The proposed procedures 1) promote sparsity, i.e., reduces sidelobes, artifacts and needs fewer measurements 2) impose energy constraints, i.e. privileges extended objects, such as tunnels, and confines the contrast function to more realistic values: resulting images are less spiky and more continuous 3) are computationally fast, easy to implement in routines, and inherently accept complex valued inputs.

ACKNOWLEDGMENT

The authors are thankful to Mr. William J. Baldygo, Air Force Research Laboratory / Sensors Directorate, and Dr. Arje Nachman, Air Force Office of Scientific Research, for sponsoring and funding this research.

REFERENCES

[1] T. J. Cui, and W. C. Chew, "Diffraction Tomographic Algorithm for the Detection of Three-Dimensional Objects Buried in a Lossy Half-Space," *IEEE Trans. Antennas Propag.,* Vol. 50, No. 1, pp. 42-49, Jan. 2002.

[2] M. S. Zhdanov, *Geophysical Inverse Theory and Regularization Problems*, Methods in Geochemistry and Geophysics, Vol. 36, Elsevier, Amsterdam, 2002.

[3] W. C. Chew, J. M. Jin, E. Michielssen, J. Song, *Fast and Efficient Algorithms in Computational Electromagnetics,* Artech House, Boston, MA, 2001.

[4] L. Lo Monte, D. Erricolo, F. Soldovieri, M.C. Wicks, "Radio Frequency Tomography for Tunnel Detection," *IEEE Transactions on Geoscience and Remote Sensing*.Vol. 48, No. 3, pp. 1128-1137, Mar. 2010.

[5] L. Lo Monte, D. Erricolo, F. Soldovieri, M. C. Wicks, "RF Tomography for Belowground Imaging of Extended Targets and Close-in Sensing" *IEEE Geoscience and Remote Sensing Letters.* In press.

[6] L. Lo Monte, L. K. Patton, M. C. Wicks, "Mitigation of Coupling in RF Tomography with Applications to Belowground Imaging," *IEEE International Radar Conference*, Washington, DC, May 10-14 2010.

[7] Y. Altuncu, I. Akduman, O. Ozdemir, A. Yapar, "Numerical Computation of the Green' Function of a Layered Media With Rough Interfaces," *Microwave & Optical Tech. Lett.,* vol. 19, no. 5, pp. 1204-1209, Mar. 2007.

[8] A. Giannopoulos, *GPRMAX Simulator,* www.gprmax.org

[9] D. W. Winters, B. D. Van Veen, S. C. Hagness, "A Sparsity Regularization Approach to the Electromagnetic Inverse Scattering Problem," *IEEE Trans. Antennas Prop.*, vol. 58, no. 1, pp. 145-154, Jan. 2010.

[10] A. Beck, M. Teboulle, "A Fast Iterative Shrinkage-Thresholding Algorithm for Linear Inverse Problems," SIAM J. Imaging Sci., vol 2, pp. 183-202, 2009.

[11] I. Loris, M. Bertero, C. De Mol, R. Zanella, L. Zanni, "Accelerating Gradient Projection Methods for L1-constrained Signal Recovery by Steplength Selection Rules," *Applied Computational Harmonic Analysis,* N. 27, pp. 247-254, 2009.

[12] S. Boyd, L. Vanderberghe, *Convex Optimization,* Cambridge University Press, Cambridge, UK, 2004.

[13] M. Çetin, W. C. Karl, "Feature-Enhanced Synthetic Aperture Radar Image Formation Based on Nonquadratic Regularization," *IEEE Trans. Image Proc.,* Vol. 10, No. 5, pp. 623-631, Apr. 2001.

[14] T. J. Kragh, A. A. Kharbouch, "Monotonic Iterative Algorithms for SAR Image Restoration," *IEEE International Conf. Image Processing,* pp. 645-648, Atlanta, CA, Oct 8-11 2006.